Computational fluid dynamic simulation of the supersonic CO2 flow during champagne cork popping

Abdessamad Benidar, Robert Georges, Vinayak Kulkarni, Daniel Cordier, Gérard Liger-Belair

Computational Fluid Dynamic simulation of the supersonic CO_2 flow during champagne cork popping

Abdessamad Benidar [1], Robert Georges [1,a)], Vinayak Kulkarni [2], Daniel Cordier [3], and Gérard Liger-Belair [3,a)]

[1] Université de Rennes, CNRS, IPR (Institut de Physique de Rennes) - UMR 6251, F-35000 Rennes, France
[2] Department of Mechanical Engineering, Indian Institute of Technology Guwahati, Guwahati, India
[3] Equipe Effervescence, Champagne et Applications (GSMA - UMR CNRS 7331), Université de Reims Champagne-Ardenne, UFR Sciences Exactes et Naturelles, BP 1039, 51687 Reims Cedex 2, France.

[a)] Authors to whom correspondence should be addressed: robert.georges@univ-rennes1.fr; gerard.liger-belair@univ-reims.fr

ABSTRACT

Behind the iconic “pop!" accompanying the uncorking of a champagne bottle hides a gas flow of surprising complexity. Its modeling is made delicate by its supersonic nature, its interaction with the cork stopper, the eminently unsteady character of the flow escaping from the bottle, and the continuous change of the geometry of the computational flow domain due to the displacement of the cork. Computational Fluid Dynamics (CFD) simulations revealed the formation, evolution and dissipation of shock wave patterns during the first millisecond following champagne cork popping. A first crown-shaped shock wave pattern develops radially, then followed by the formation of a detached shock wave, or bow shock, induced by the presence of the cork in the axial path of the supersonic gas flow. Moreover, the good agreement between the position of the bow shock previously observed through high-speed imaging and that determined through CFD simulations argues in favor of the numerical method used to describe the ejection of the gas mixture expelled from the bottleneck immediately after the cork popping process.

I. INTRODUCTION

Nowadays, after more than three centuries and undergoing continuous refining, champagne has undoubtedly become the most renowned French sparkling wine, praised world-wide for the fineness of its carbon dioxide (CO_2) bubbles.[1] Indeed, during champagne making, bottles reach a high pressure because gas-phase CO_2 forms together with ethanol during a key step, the in-bottle fermentation process promoted by adding yeasts and sugar in bottles hermetically sealed with a cork stopper.[1] This is actually the application of Henry's law which states that the concentration of dissolved CO_2 in the liquid phase is proportional to the partial pressure of gas-phase CO_2 in the bottleneck. Moreover, because the solubility of CO_2 in the liquid phase is strongly temperature-dependent (the lower the temperature of the wine, the higher the gas solubility), the partial pressure of gas-phase CO_2 in the bottleneck is therefore also strongly temperature-dependent (the lower the temperature of the wine, the lower the partial pressure of gas phase CO_2). Since the driving force behind the cork popping process is the force exerted by gases under pressure in the bottleneck on the base of the cork stopper, the cork popping velocity is therefore, definitely influenced by the champagne temperature, as already shown in a previous article.[2]

During the cork popping process, concomitantly with the cork stopper being expelled from the bottleneck under the action of pressure, a plume composed of a gas mixture mainly of CO_2 (with traces of water vapor) freely expands out of the bottleneck through the ambient air and then experiences adiabatic cooling.[3–5] High-speed video imaging was used recently to visualize champagne cork popping, and especially the condensation processes following the adiabatic expansion of the gas mixture. Transparent champagne bottles of different temperatures were used in those experiments.[5] The temperature of the bottles (and therefore their inner pressure) was found to be a key parameter concerning the condensation processes that can occur just above, and inside the bottlenecks. Most interestingly, for the bottles stored at 20 °C (under a pressure close to 7.5 bar), the characteristic grey-white cloud of fog classically observed above the bottlenecks of bottles stored at lower temperatures was replaced by a more evanescent plume, surprisingly blue, starting from inside the bottleneck.[5] Since the saturation ratio experienced by gas-phase CO_2 in the adiabatic expansion has strong temperature dependence, it was emphasized that the blue haze is the signature of a partial and transient heterogeneous freezing of gas phase CO_2 on ice water clusters, homogeneously nucleated in the bottlenecks.[5] Even more recently, a

comparison between the condensation phenomena accompanying cork popping from bottles stored at 20 and 30 °C was made.[6] The initial bottleneck-to-ambient-pressure ratio (7.5 for the bottles stored at 20 °C, compared to about 10 for those stored at 30 °C) much exceeded the critical ratio needed for the CO_2/H_2O gas mixture to reach Mach 1. In these cases, under-expanded supersonic jets got expelled from the throat of the bottlenecks. Moreover, during the very first millisecond following the cork popping process, evanescent normal shock waves were identified in the plumes, until the reservoir-to-ambient-pressure ratio went below a critical value needed for their formation, which were *de facto* seen vanishing.[6]

In fact, the expansion of a high-pressure gas due to sudden exposure to a low-pressure environment gives rise to a so-called free jet, as opposed to a jet confined by the walls of a duct. The free jet acquires supersonic speed when the sonic state gets reached at the outlet that separates the high- and low-pressure areas. This condition is met when the ratio of the upstream and downstream pressures is greater than approximately 2 (the precise value depends on the ratio of the specific heats of the gas). Such free jet can reach very high Mach number, which corresponds to high speed and extremely low temperature, may be close to absolute zero,[7] under the principle of energy conservation. This specificity of supersonic flows is used in particular to carry out studies of chemical reactivity[8] or spectroscopy[9] at very low temperature in the gas phase. The interaction of the supersonic free jet with the downstream static gas leads to the formation of a complex network of shock waves, also called diamond shocks, as named by Ernst Mach who first described them using shadowgraphy.[10,11] It may be noted that, at high pressure ratios, a normal shock wave or Mach disk forms, perpendicular to the flow direction, after passing through which the gas attains subsonic state. Such a shock wave occurs at the outlet of Laval nozzles which propel rockets, missiles or scramjets and also the eruption of a volcano,[12–14] or during the formation of geysers observed on the surface of the Europa satellite.[15] The location of Mach disk formation is downstream from the gas outlet for a given higher value of governing pressure ratio.[16] The position of the Mach disk remains stationary as long as the upstream and downstream pressures do not change over time, which is not the case if the volume of the high pressure gas is finite, as is the case for a shock tube[17] or for gas escaping from a bottle of champagne. Therefore, while performing simulations for such expansion, it is necessary to account the finite nature of the high pressure reservoir[18] and unsteadiness of flow. An

additional difficulty for the flow from the bottle of champagne is the presence of the cork stopper as an obstacle, to which the flow would be impacting. A detached shock wave[19] gets formed when a supersonic flow hits a surface. As a result of this, the gas adopts low speed and high pressure condition after passing through the shock wave. This situation is very similar to the cold spray process where particles are ejected at supersonic speed which then collide with the substrate to be treated.[20] In this case, two shock waves interfere: a free jet based network and a detached shock wave upstream of the substrate. These flow complications are indeed present in the champagne cork popping process. Here, the gas mixture expelled from the bottleneck must adapt to the ambient pressure through a network of shock waves but also must face the presence of the cork that is in its path. Nevertheless, a significant difference from the cold spray study by Pattison *et al*.[20] is that the distance between the gas outlet (the bottleneck) and the obstacle (the flying cork) varies over time.

The present study addresses the aforementioned issues by considering the champagne cork popping process as a supersonic free jet expelled from a finite reservoir and impacting a moving obstacle. Flow field comprised of the shock structure experienced by the gas flow, expelled at supersonic speed from the champagne bottleneck, after ejection of the cork stopper, is analyzed with time using Computational Fluid Dynamics (CFD). The calculation performance and the stability of the two-dimensional axisymmetric method used were evaluated by comparing the numerical results of the transient gas expansion with the normal shock wave position previously observed through high-speed video imaging.[5,6]

II. METHODS

A. Computational domain and initial conditions

Commercial solver ANSYS Fluent is used for present studies. The axisymmetric geometry approximation was chosen because it is well suited to the axial symmetry of the flow field corresponding to the gas ejection during champagne cork popping from a bottle held vertically. The calculation domain (Fig. 1) includes the internal gaseous volume of approximately 35 cm^3, under pressure, found within the bottleneck of the champagne sealed bottle (i.e., the gas phase between the liquid surface and the cork stopper). This gas

mixture consists of gas-phase CO_2, with traces of water vapor, nitrogen, ethanol vapor and a myriad of other volatile compounds.[1] Nevertheless, the partial pressure of gas-phase CO_2 is largely dominant compared with that of all other gaseous compounds.[1] Therefore, for the sake of simplicity, the numerical simulations were carried out by considering pure CO_2 in the gas phase under pressure in the bottleneck of the corked bottle. Moreover, the initial pressure and temperature were set at 7.5 bar and 20 °C respectively, in order to comply with one of the experimental conditions imposed in previous studies.[5,6] The current simulations are based on the exact geometric profile of a bottle of champagne (the radial/axial coordinates of the exact geometry of the bottleneck is included as supplementary material). In the headspace, the section of the bottleneck gradually reduces until it reaches an internal diameter close to 1.8 cm at the outlet of the bottle. The other part of the calculation domain is the external environment formed by the ambient air in which the CO_2 would freely expand.

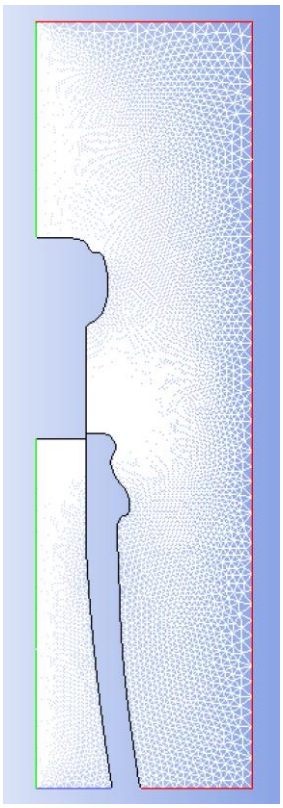

FIG. 1. Mesh of the computational domain at initial time.

The movement of the champagne cork was controlled with a user-defined function (UDF) imported from the ANSYS Fluent software. In this function, the ejection speed of the cork stopper is fixed at 18.6 $m.s^{-1}$ (Fig. 2), as determined from a previous set of experimental observations conducted under the same flow conditions[6] (Fig. 3). These preliminary experiments proved to be essential to determine the speed of movement of the plug and thus to impose a realistic temporal evolution of the contour of the simulated flow field. It is noteworthy to mention that the elasticity of the cork stopper (visible on the experimental time sequence presented in Fig. 3) was not taken into account in the present simulations for the sake of simplicity. This is the reason why the base of the cork did not adopt the typical mushroom shape of a champagne popped cork but remained cylindrical once expelled from the bottleneck (as shown in Figs. 4 and 5).

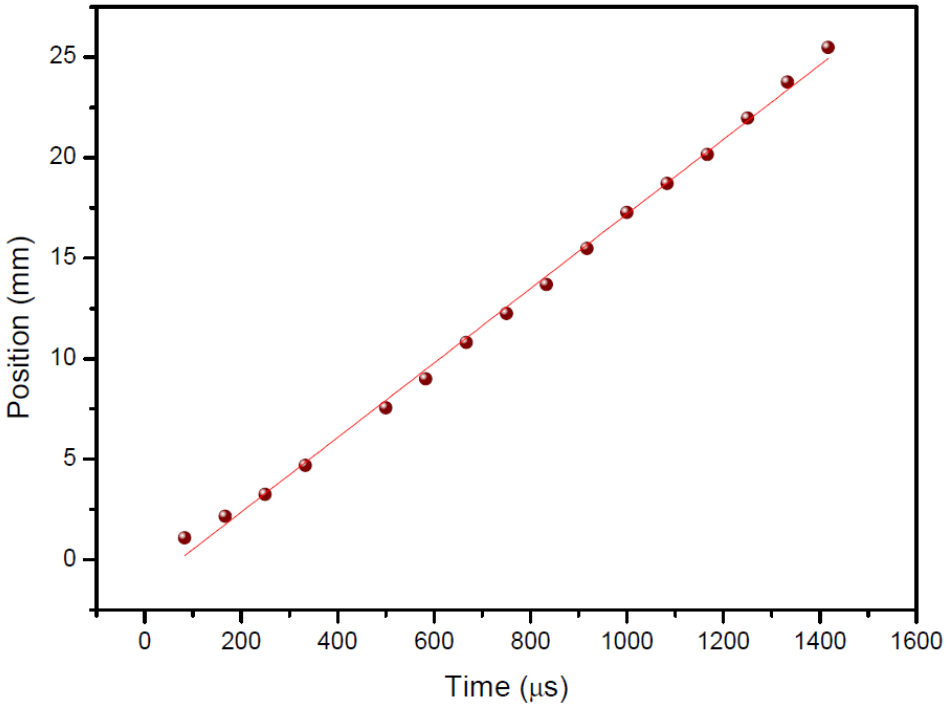

FIG. 2. Position of the cork stopper as a function of time. The successive positions of the rear part of the cork stopper result from our experimental observations conducted on the dynamics of cork popping from a bottle initially kept at 20 °C, with an inner pressure of 7.5 bar.[6]

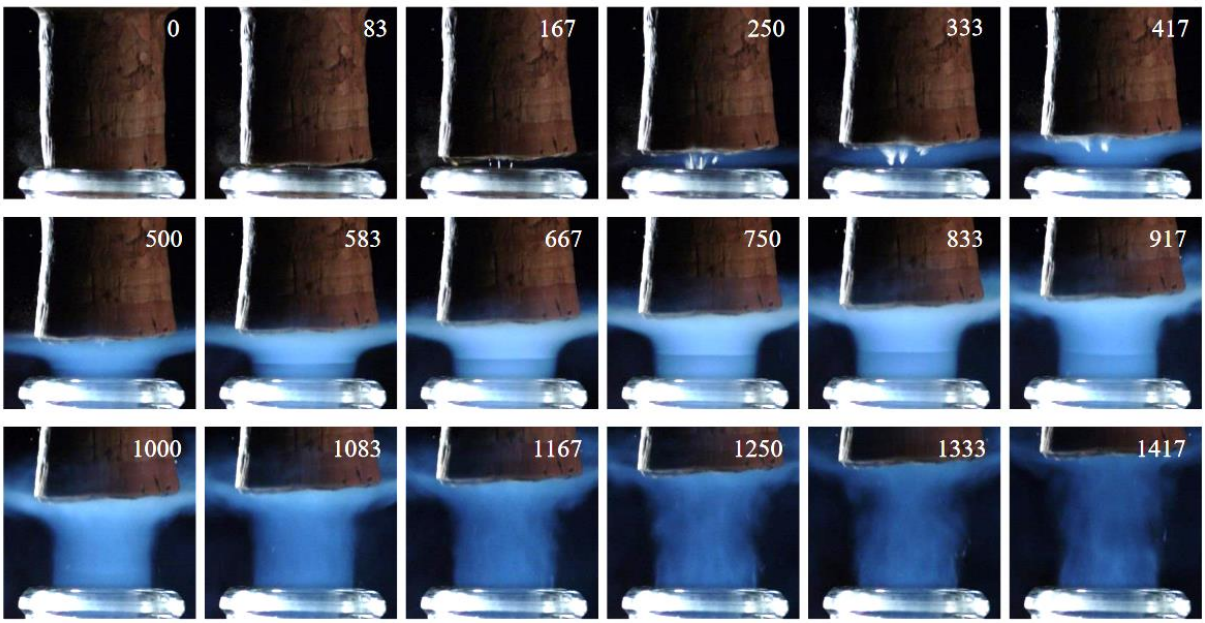

FIG. 3. Time sequence showing details of the cork popping expelled from the bottleneck of a bottle stored at 20 °C, as captured through high-speed imaging.[6] The time elapsed after cork popping appears in each frame (in μs).

B. Calculation method.

Our fluid dynamics calculation study was based on the commercial ANSYS Fluent software. More specifically, in the present study, Navier-Stokes axisymmetric equations and species transport equations (Eq.1) were used in the finite volume formulation along with the mixing form for all the flow variables.

$$\frac{\partial U}{\partial t}+\frac{\partial F_I}{\partial x}+\frac{\partial G_I}{\partial y}+S+(S_I-S_v)=\frac{\partial F_v}{\partial x}+\frac{\partial G_v}{\partial y} \qquad (1)$$

Where,

$$U=\begin{pmatrix}\rho\\ \rho u\\ \rho v\\ \rho E\\ C_1\\ .\\ .\\ C_{N-1}\end{pmatrix} \qquad F_I=\begin{pmatrix}\rho u\\ \rho u^2+p\\ \rho uv\\ (\rho E+p)u\\ uC_1\\ .\\ .\\ uC_{N-1}\end{pmatrix} \qquad G_I=\begin{pmatrix}\rho v\\ \rho uv\\ \rho v^2+p\\ (\rho E+p)v\\ vC_1\\ .\\ .\\ vC_{N-1}\end{pmatrix}$$

$$F_v = \begin{pmatrix} 0 \\ \tau_{xx} \\ \tau_{xy} \\ u\tau_{xx} + v\tau_{xy} - q_x - \sum_{i=1}^{N} h_i C_i \bar{u}_i \\ -C_1 \bar{u}_1 \\ . \\ . \\ -C_{N-1}\bar{u}_{N-1} \end{pmatrix} \qquad G_v = \begin{pmatrix} 0 \\ \tau_{xy} \\ \tau_{yy} \\ u\tau_{xy} + v\tau_{yy} - q_y - \sum_{i=1}^{N} h_i C_i \bar{v}_i \\ -C_1 \bar{v}_1 \\ . \\ . \\ -C_{N-1}\bar{v}_{N-1} \end{pmatrix}$$

$$S = -\begin{pmatrix} 0 \\ 0 \\ 0 \\ 0 \\ S_1 \\ . \\ . \\ S_{N-1} \end{pmatrix} \qquad S_I = \frac{1}{y}\begin{pmatrix} \rho v \\ \rho uv \\ \rho v^2 \\ (\rho E + p)v \\ vC_1 \\ . \\ . \\ vC_{N-1} \end{pmatrix}$$

$$S_v = \frac{1}{y}\begin{pmatrix} 0 \\ \tau_{xy} - \frac{2}{3} y \frac{\partial(\mu v/y)}{\partial x} \\ \tau_{yy} - \tau_{\theta\theta} - \frac{2}{3}\mu\left(\frac{v}{y}\right) - \frac{2}{3} y \frac{\partial(\mu v/y)}{\partial y} \\ u\tau_{xy} + v\tau_{yy} - q_y - \frac{2}{3}\frac{\mu v^2}{y} - \frac{2}{3} y \frac{\partial(\mu v^2/y)}{\partial y} - \frac{2}{3} y \frac{\partial(\mu uv/y)}{\partial x} - \sum_{i=1}^{N} h_i C_i \bar{v}_i \\ -C_1 \bar{v}_1/y \\ . \\ . \\ -C_{N-1}\bar{v}_{N-1}/y \end{pmatrix}$$

Here, U is the solution or conservative vector, F_I, G_I and F_v, G_v are convective and viscous flux vectors in x and y directions respectively, S is the reaction source term, S_I and S_v represent the inviscid and viscous source terms respectively. Besides, ρ is density, μ is dynamic viscosity, T is temperature, p is pressure and u and v are the velocities in x and y directions respectively. Here, total energy is represented as E $\left(E = e + \frac{1}{2}(u^2 + v^2)\right)$ where, e is internal energy $\left(e = \sum_{i=1}^{N} e_i \frac{C_i}{\rho MW_i}\right)$. Here, e_i is the molar internal energy of the species $\left(e_i = h_{f_i}^0 + \int_{T_R}^{T} C_{pi} dT - R_u T\right)$. Where, C_i, MW_i, $h_{f_i}^0$ and C_{pi} represent the mass concentration, molecular weight, heat of formation and specific heat at constant pressure,

respectively. Further, R_u is the universal gas constant, and 'N' is number of species. The stress terms are $\tau_{xx} = \mu\left(\frac{4}{3}\frac{\partial u}{\partial x} - \frac{2}{3}\frac{\partial v}{\partial y}\right)$, $\tau_{xy} = \mu\left(\frac{\partial u}{\partial y} + \frac{\partial v}{\partial x}\right)$, $\tau_{yy} = \mu\left(\frac{4}{3}\frac{\partial v}{\partial y} - \frac{2}{3}\frac{\partial u}{\partial x}\right)$ and $\tau_{\theta\theta} = \mu\left[\frac{-2}{3}\left(\frac{\partial u}{\partial y} + \frac{\partial v}{\partial x}\right) + \frac{4v}{3y}\right]$. Here, $\bar{u}$ and $\bar{v}$ represent the diffusion velocities in x and y direction respectively and are calculated by using the Fick's law, i.e. $Y_i\bar{u} = D_{im}\frac{\partial Y_i}{\partial x}$, $Y_i\bar{v} = D_{im}\frac{\partial Y_i}{\partial y}$, where D_{im} is treated as a constant. In the current studies, flow is non-reacting hence the production rate of each species would be zero. This commercial solver accounts kinetic theory based ideal gas law for calculation of viscosity and thermal conductivity.

The k-epsilon turbulence model ("Realizable" option) along with the Near-Wall Treatment ("Enhanced Wall Treatment" option) was considered for present simulations. This turbulence model along with the kinetics theory based mixture diffusion coefficients help to simulate the turbulent flow effectively. The "pressure-velocity coupling" algorithm was chosen for the calculation process. The "PRESTO" model was applied for the discretization of the pressure and to obtain a good precision of the pressure gradients near the walls. The "Second Order Upwind" scheme was selected for the inviscid flux computations. Considering the cork stopper velocity and the Courant-Friedrichs-Lewy (CFL) condition, the computational time interval or time step was set to 10^{-6} s, and the maximum number of iterations for each time step was set to 200. The external boundary of the computational domain was maintained at ambient temperature and pressure.

C. Dynamic mesh.

The computational domain gets modified due to the ejection of the cork stopper. Therefore, it was necessary to use a dynamic mesh to simulate the gas flow throughout the ejection of the cork stopper. Smoothing and remeshing methods were used and properly parameterized to maintain a high mesh quality and avoid any degeneration or deformation of the grid during its updation and hence throughout the calculation process. The diffusion-based smoothing method was adopted for the mesh deformation with a limit distance and a diffusion parameter set to 0.1. The local remeshing method was employed when the mesh violated the skewness or size criteria.[21] The minimum and maximum length scales parameters were set to 10^{-6} m and 0.002 m, respectively, and the maximum cell skewness fixed at 0.7.

III. RESULTS AND DISCUSSION

A. Shock wave pattern

According to gas dynamics and as confirmed by our simulations shown in Fig. 4, the gas escaping from the bottle reaches a supersonic regime. Before describing the detailed flow field, we shall briefly recall some basics of compressible flow.[22] Two conditions have to be met by the gas flow to break the sound barrier. The first one relates to the existence of a throat, i.e. a spatial zone delimiting a converging duct area from a diverging one. Due to mass conservation, a subsonic flow needs to move in a converging duct for acceleration. Conversely, the decrease of density of a supersonic flow is so rapid that it can no longer be compensated by the velocity increase to maintain its mass flow ($\dot{m} = \rho AV$). Both velocity (V) and area (A) must increase to compensate for the density (ρ) decrease of a supersonic flow. It follows that the speed of sound can only be reached if the gas flow passes through a throat. The shoulder of the bottle of champagne behaves as a converging duct whereas the diverging one is only virtual. It corresponds to the large atmospheric volume in which the high-pressure gas is "freely" discharged once the cork has popped. The second condition to reach a supersonic regime is that the flow must reach the speed of sound at the throat, which then acts like a sonic throat characterized by unit Mach number; this condition is called choked flow. If this condition is not satisfied, the gas will decelerate downstream from the throat. A choked flow is obtained provided the gas reaches the critical pressure p^* at the throat which is given by the isentropic choking pressure ratio $\frac{p^*}{p_0} = \left(\frac{2}{\gamma+1}\right)^{\frac{\gamma}{\gamma-1}}$, where p_0 is the pressure prevailing in the bottle and where γ denotes the specific heat ratio of the gas. Thus, a supersonic flow develops provided that $p^*/p_0 \sim 0.5$, or equivalently, that the nozzle pressure ratio (NPR) $p_0/p^* \sim 2$.

As the initial pressure of a bottle of champagne far exceeds two atmospheres, it is certain that the gas it contains will reach a supersonic regime when discharging into the atmosphere. This is well confirmed in our CFD simulations (Fig. 4 (500 μs) and Fig. 5 (518 μs)) where the complex shock wave pattern (shock diamonds), very specific to supersonic flows and first described by Mach,[10] is clearly visible.

The CFD simulations reveal that cork popping is followed by successive flow phases and the reader should refer to the simulation rows shown in Fig. 4 corresponding to 500, 917

and 1167 µs, respectively, as well as to the evolution of the Mach number of the gas versus time presented in Fig. 5 from 166 to 1577 µs.

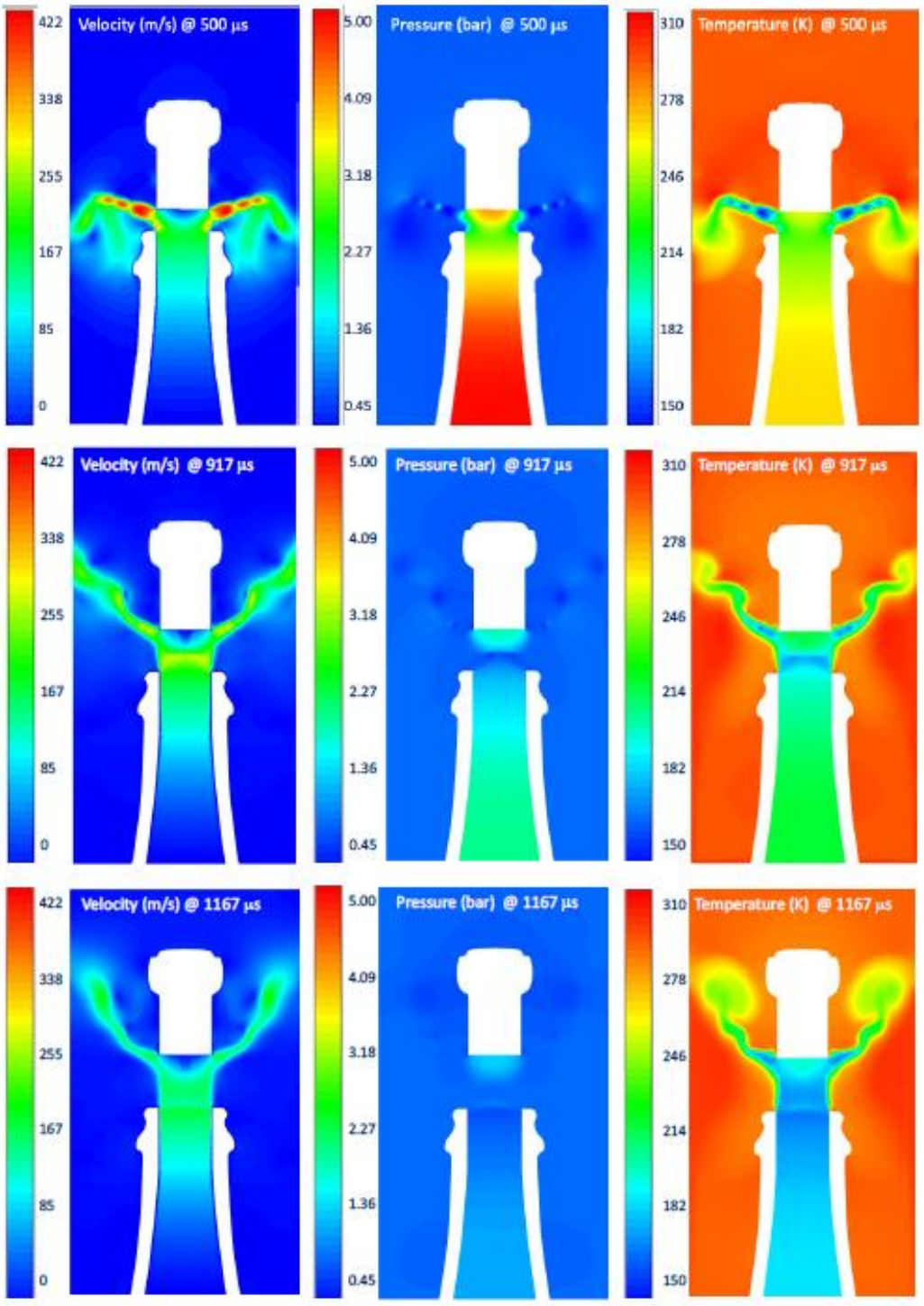

FIG. 4. Simulation of pure CO_2 expanding freely into ambient air (20°C, 1.013 bar) following the cork popping of a champagne bottle initially kept at 20 °C with an inner pressure of 7.5 bar. The first, second and third panel rows relate to flow times of 500,

917 and 1167 μs respectively, measured after the cork popping. The first, second and third panel columns are relative to the flow velocity, static pressure and temperature, respectively.

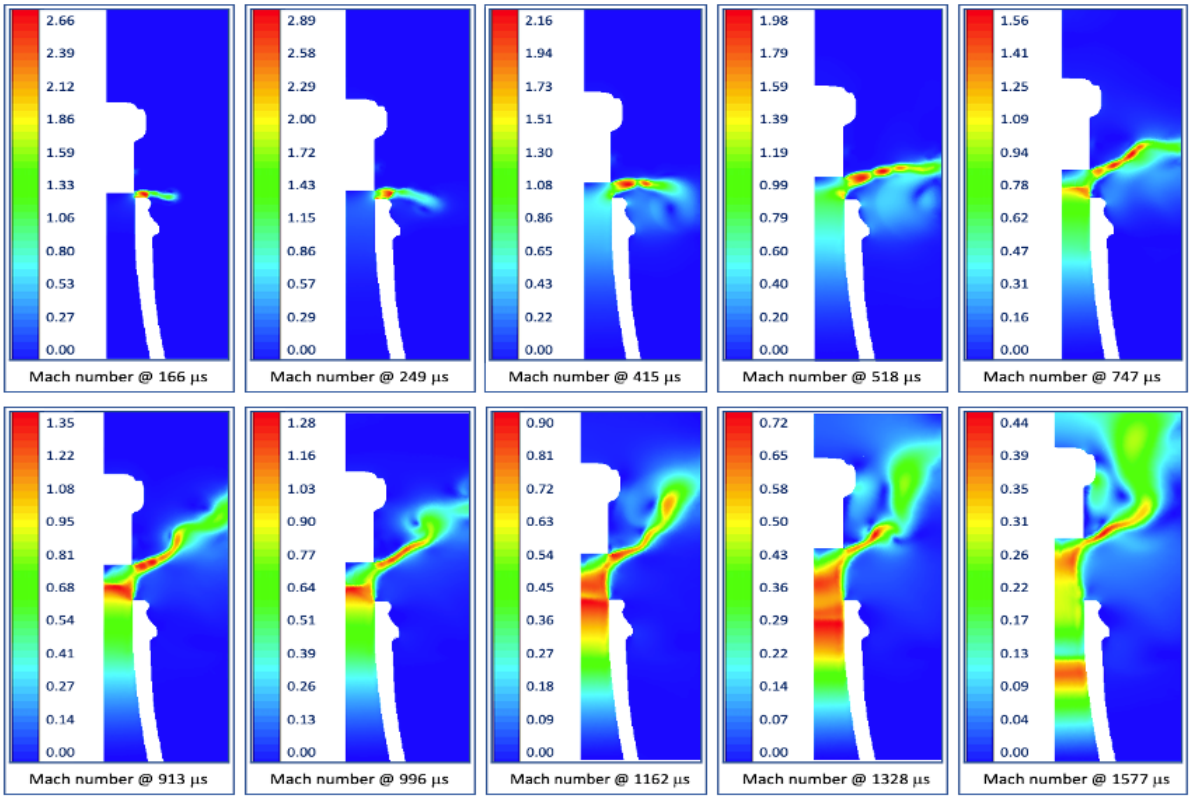

FIG. 5. Simulation of the Mach number versus time of pure CO_2 expanding freely into ambient air following cork popping. The bottle is initially kept at 20 °C and 7.5 bar. The first seven images of the series reveal the supersonic character of the flow (Mach> 1) whereas it is subsonic (Mach <1) from the eighth image because the pressure in the bottle has become subcritical (note that the Mach number scale has been adapted for each panel to increase plot contrast).

During the early phase closely following cork ejection (for example for a flow time of 500 μs as shown in Fig. 4; see also Fig. 5 (166, 249, 415 and 518 μs)), the cork is so close to the throat of the bottleneck that the pressure of the gas located between the cork and the bottle is still several bars, much higher than the required critical pressure. Therefore, the flow comprised in the small volume between the bottleneck and the cork stopper is not

choked while flowing along the bottle axis and hence remains in subsonic state. The gas is accelerated until it reaches a maximum speed of about 200 $m.s^{-1}$ at the bottleneck. This speed corresponds to a Mach number of 0.78 (Fig. 6) which indicates that the speed of sound has not yet been reached at the bottleneck. This results in deceleration of the gas after the bottleneck to zero speed at the cork. Interestingly, the temperature of the gas at the bottleneck drops to -43 °C before rising to -10 °C at the cork, thus it explains the formation of water ice observed on the internal face of the cork during this initial phase of ejection.[6] The high pressure gas in the region under the cork has no alternative but to escape laterally into atmospheric air giving rise to a nice crown shaped supersonic expansion characterized by a typical succession of shock cells along which the expanding gas gradually equilibrates its static pressure to ambient pressure. Although the lateral diamond shocks were not revealed by the high speed camera,[5,6] their presence seems to be confirmed by another numerical simulation.[23] From Fig. 5, it can be seen that the Mach number of the supersonic jet crown reaches about 2.9 in the very early stage of the lateral gas expansion (< 249 μs).

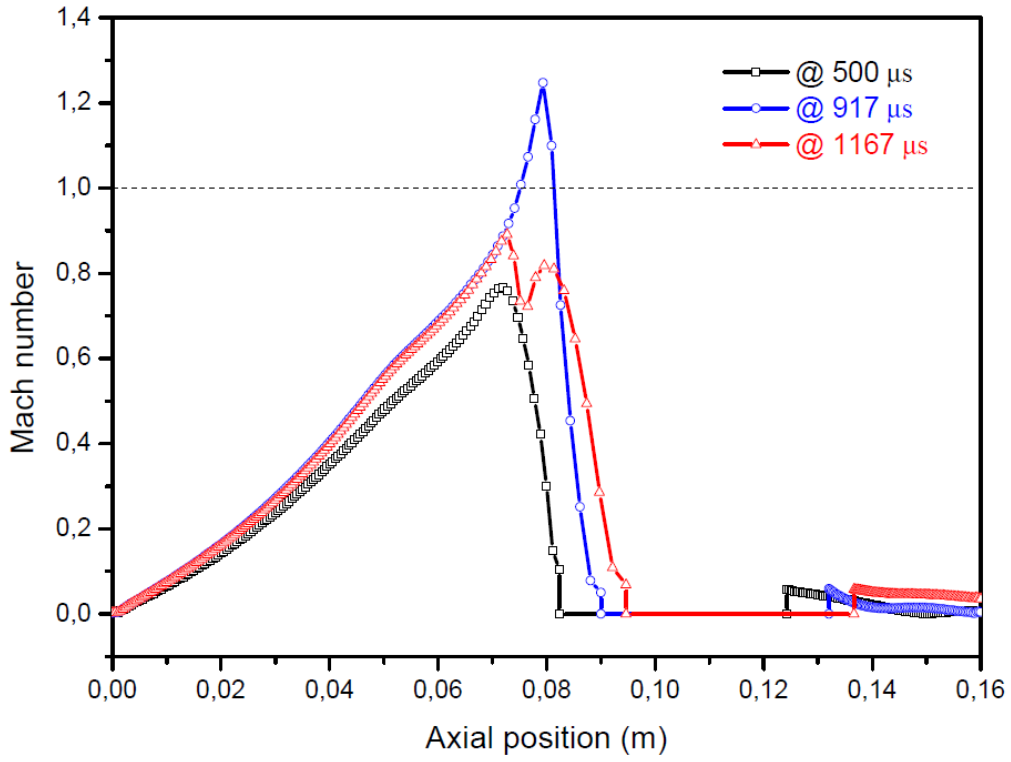

FIG. 6. Mach number axial profile of a gas escaping from a bottle initially at 20°C and 7.5 bar for flow time of 500, 917 and 1167 μs. At 500 μs (phase 1) the exit pressure is too high so that the gas flow is not choked along the bottle axis, hence it decelerates downstream of the bottleneck. At 917 μs (phase 2), the flow is supersonic and a detached shock is forming in front of the cork. At 1167 μs (phase 3), the pressure in the bottle is too low and nozzle pressure ratio (NPR) is not high enough to maintain a choked flow on the bottle axis.

A second phase begins once the cork goes far enough from the bottleneck so that the pressure downstream is lower than the critical value. In that case, the bottleneck acts as a sonic throat and the gas flow is accelerated downstream to reach supersonic speeds up to Mach 1.6-1.8 (see second row of Fig. 4, relative to 917 μs; see also panels 747, 913 and 996 μs of Fig. 5). The enthalpy of the gas is converted into kinetic energy leading to a drop in temperature down to -95°C thus triggering the condensation of CO_2, as observed in our previous work.[6] The fluid molecules then impinge on the cork face and rebound. This interaction leads to the formation of a bow shock which can be seen as the coalescence of reflected signals by the object. The shock is a compression front across which the flow properties jump. According to the second law of thermodynamics, a flow behind a normal shock wave is necessarily subsonic[22]. The distance between the bow shock and the object, i.e. the thickness of the shock layer, depends on the Mach number and cannot be determined using a simple analytical expression. It needs to be determined by numerical calculation methods such as those used in the present work.

As confirmed by our simulations, the flow behind the shock wave is subsonic, its temperature being raised close to −60°C and the gas is recompressed to about 2.2 bar so that it further expands laterally to reach a supersonic regime responsible for the formation of lateral shock cells. The simulations clearly show that the radial ejection of the gas during the initial phase (phase 1) is followed by a purely axial ejection once the normal shock wave is formed at the bottle outlet (phase 2). Gas escapes laterally only after passing through the shock wave and impacting on the plug.

During the third phase, the pressure of the gas in the bottle has become too low to maintain an NPR > 2, the choked conditions are no longer satisfied, neither at the bottleneck nor at the edge of cork. The normal shock wave and the crown shaped lateral shock cells can

no longer form (see last row in Fig. 4 corresponding to a flow time of 1167 µs; see also Fig. 5 for times greater than 996 µs). The flow is now subsonic and a rarefaction wave propagates in the bottleneck.

B. Position of the detached shock

Figure 7 shows the evolution of the calculated position of the bow shock as a function of the pressure in the bottle (the open symbols correspond to the position of the rarefaction wave which propagates inside the bottleneck). The position of the bow shock is compared to the position of the Mach disk that would ideally form if the jet did not hit the cork, which is of course only an abstraction. The position of the Mach disk is calculated from the study of Orescanin *et al*.[18] on free jets issuing from finite reservoirs. This X_{Mach} position depends on the ratio between the high pressure of the reservoir (p_0) and the external pressure (p_{ext}), for pressure ratios less than 15. It is given by the relation $\frac{X_{Mach}}{D} = 0.41\left(\frac{P_0}{P_{ext}}\right)^{0.66}$, where *D* is the diameter of bottle outlet. The Mach disk gets closer as gas escapes and the cylinder pressure drops. However, it remains much further from the opening of the bottle than the bow shock, which shows that it is the cork that controls the formation of the shock waves.

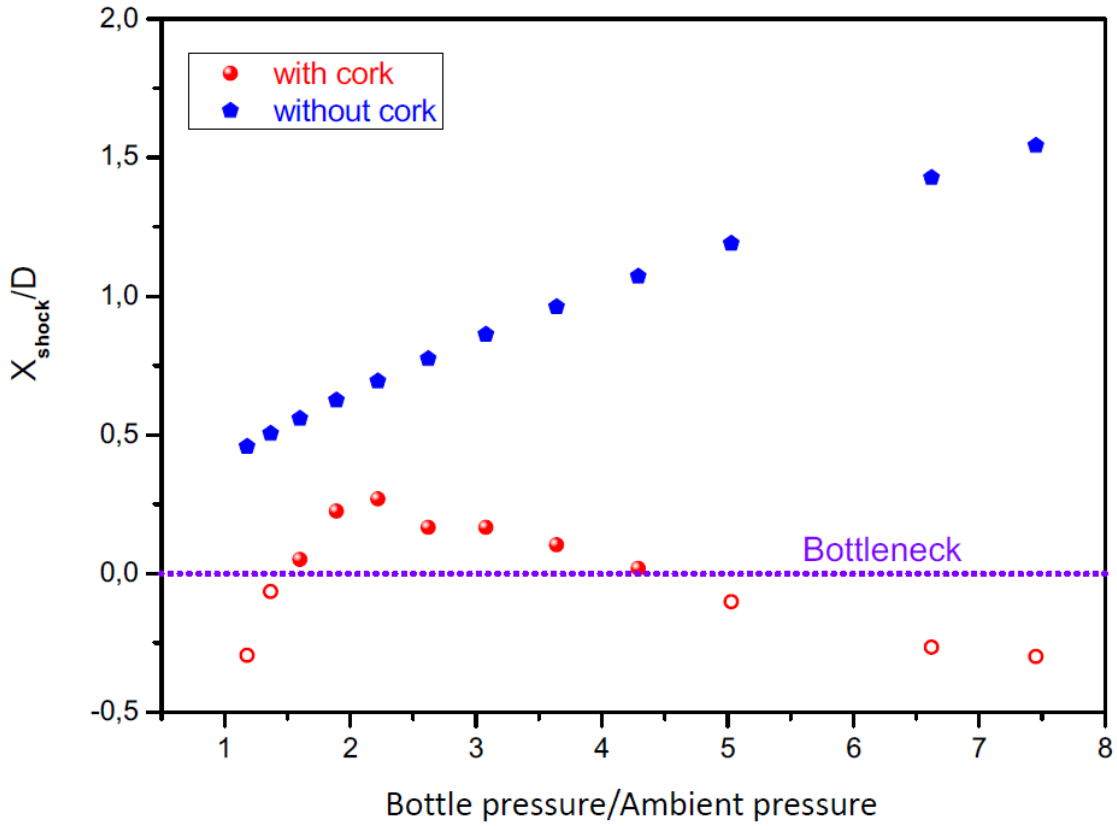

FIG. 7. Comparative position of the Mach disk and the bow shock. Blue dots: position of the Mach disk which would form in the absence of a cork during the discharge of gas into the atmosphere. Red dots (full symbols): simulated position of the bow shock. Red dots (open symbols): simulated position of the rarefaction wave.

Actually, The normal shock wave could be observed experimentally (as seen in Fig. 2) due to the ambient light scattered by the water ice particles and in certain conditions by the solid CO_2 particles whose formation is triggered by the very low temperature reached by the supersonic flow during its adiabatic cooling.[5,6] By considering a Mach number $M \approx 2$ at 518 µs for a bottle initially kept at T_0 =20°C and p_0 =7.5 bar (as seen Fig. 5), an estimation based on the standard isentropic equations $p/p_0 = (T/T_0)^{\frac{\gamma}{\gamma-1}} = \left(1/\left(1+\frac{\gamma-1}{2}M^2\right)\right)^{\frac{\gamma}{\gamma-1}}$, leads to a jet temperature close to -90°C for a jet pressure of 1 bar (by considering the expelled gas mixture as pure CO_2 with a specific heat ratio $\gamma = 1.3$). Such conditions correspond indeed to the solid phase of CO_2 as discussed in the articles by Liger-Belair *et al*.[5,6]

The calculated distance of the shock wave from the cork is generally in good agreement with the observations, with nevertheless a better agreement for longer flow times (Fig. 9). These small disagreements could be explained by the presence of the condensation of water and CO_2 molecules which is not taken into account in our CFD simulations although responsible for an important release of heat of condensation in the flow. Not surprisingly, the shock detachment distance reduces when the Mach number increases, i.e. with increasing bottle pressure. Although difficult to model and predict, it is a well-known effect observed in many studies of gas dynamics.[19,24] Additional simulations were performed for lower initial pressure conditions of 3, 5 and 6 bar (Fig. 10). They do confirm observations: the normal shock wave is closer to the cork stopper as the upstream pressure increases.

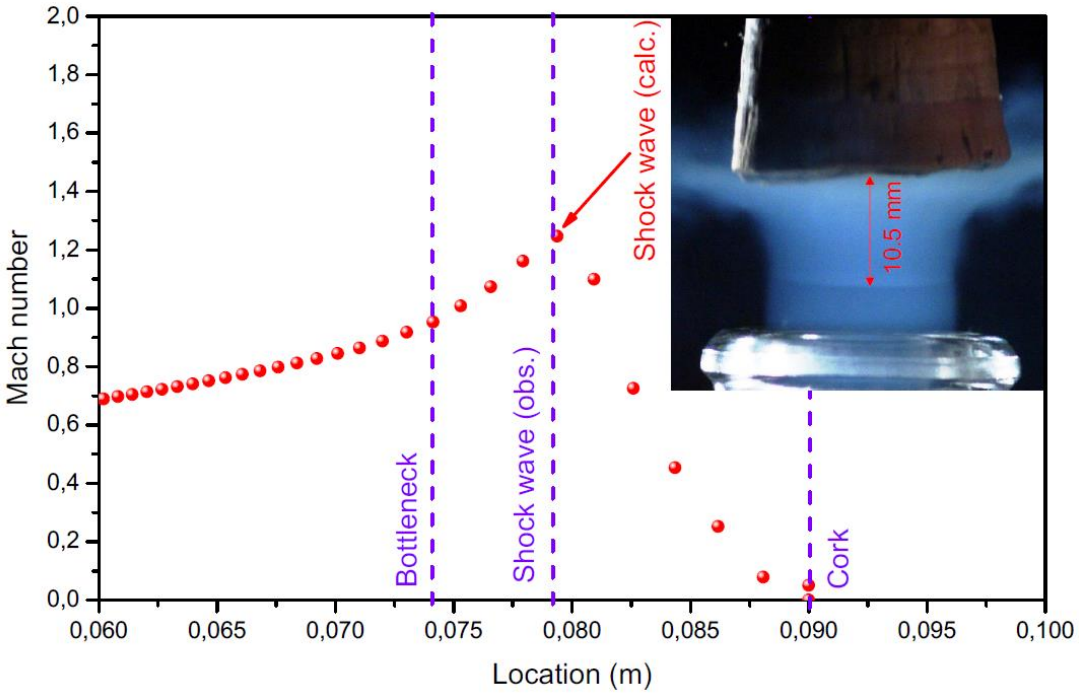

FIG. 8. Calculated and observed positions of the normal shock wave. Here, the bottle was initially kept at 20°C and 7.5 bar. Both simulation and picture correspond to a flow time of 917 µs after the cork popping. The origin of the x-axis corresponds to the surface of the liquid in the bottle.

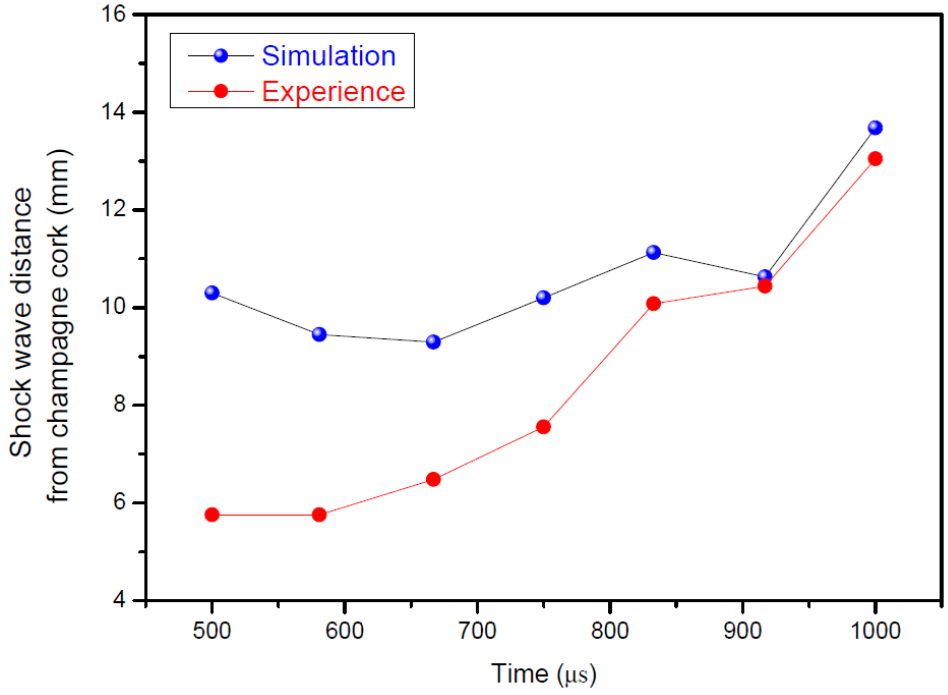

FIG. 9. Temporal evolution of the calculated and observed positions of the detached shock wave forming in front of the cork.

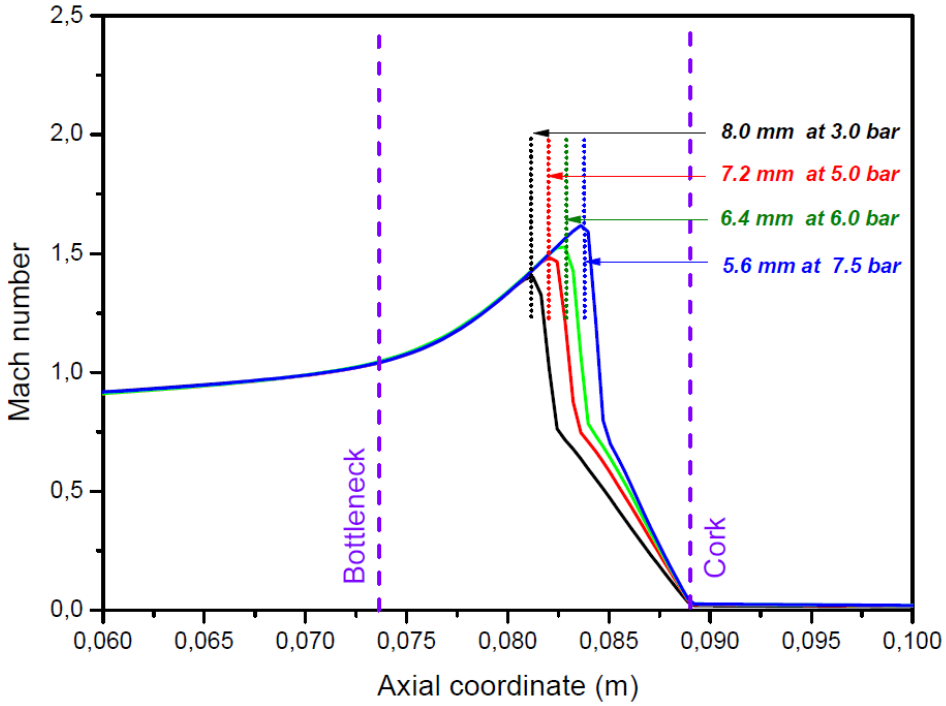

FIG. 10. Calculated positions of the detached shock wave for different initial bottle pressures ranging from 3.0 to 7.5 bar. In the present simulations, the pressure in the bottle was kept constant and the distance between the outlet of the bottle and the cork was kept at a fixed position. It is noted that the higher the Mach number, the closer to the cork, the shock forms.

As shown in Figures 8 and 9, the calculation in three-dimensional geometry reproduces the temporal evolution of the position of the normal shock wave with good precision. Moreover, as shown in Figure 7, the presence of the plug has a determining action on the position of the normal shock wave which is more akin to a detached shock wave than to a Mach disk typical of underexpanded free jets.

IV. CONCLUSIONS

Present CFD simulations reveal the existence of three distinct flow phases following the cork popping of a bottle of champagne. In the early phase, between approximately 0 and 600 µs (time 0 corresponding to the precise moment when the cork stopper separates from the bottleneck), the gas which leaves the bottle is axially blocked by the cork. The situation is

then very different from a gas which would escape freely from a high-pressure reservoir into the atmosphere. In the case of an unobstructed free stream downstream, the gas outlet would behave like a sonic throat, causing the gas to accelerate beyond the speed of sound. In the presence of the stopper and during this initial phase, the gas which escapes from the bottle does not have the possibility of expanding sufficiently along the axis of the cylinder, so that the Mach number at the bottleneck remains less than 1. The neck of the bottle therefore does not act like a sonic throat: the gas reaches its maximum (subsonic) speed at the bottleneck after its acceleration under the effect of the progressive narrowing of the outlet section of the bottle, then decelerates downstream of the bottleneck under the effect of the sudden increase in the outlet section. In this first phase of the process, the gas located between the cork stopper and the bottle outlet is characterized by a pressure of several bars and it will obviously seek to balance its static pressure with atmospheric pressure by escaping laterally through the annular space which grows as the cork is ejected. Numerical simulations show that this space actually acts as an annular sonic throat. The gas escapes radially at supersonic speed, balancing its pressure through a succession of normal and oblique shock waves forming the usual structure of diamond shock waves clearly visible in the simulations (see Figs. 4 and 5). Note that the axial symmetry of the bottle leads to a crown-shaped supersonic expansion.

In a second phase, typically between 600 and 1000 µs, the gas pressure at the bottle outlet has become low enough for the critical condition (Mach 1) to be reached at the bottleneck (see e.g. Fig. 6). Gas then escapes from the bottle at supersonic speed, this time directed along the axis of the cylinder. The gas then impacts the cork stopper and becomes subsonic again passing through a detached shock (bow shock) induced by the presence of the cork stopper. The predicted position of this bow shock wave agrees well with the observations. It must be underlined that this shock wave corresponds to a bow shock rather than the characteristic Mach disk of non-adapted free jets that would form further away in the absence of a cork stopper.

Finally, in the last phase, typically beyond 1000 µs, the pressure in the bottle is too low to maintain the critical pressure at the bottleneck. The gas leaves the bottle at subsonic speeds and then decelerates downstream. The simulations clearly show the propagation of a rarefaction wave inside the bottle during this last phase.

Finally, let us note that this work aimed at deciphering the champagne cork popping processresents strong similarities with the ejection of gas of propulsion ejected by an aerospace launcher. The ground which moves away from the launcher as it rises in the air then plays the role of the champagne cork on which the ejected gases impact. Similarly, combustion gases ejected from the barrel of a gun are thrown at supersonic speeds onto the bullet. These problems are faced with the same physical phenomena and could be treated using the same approach.

SUPPLEMENTARY MATERIAL

See supplementary material for the initial grid of calculation outside and inside the bottleneck.

AUTHOR DECLARATIONS

Conflict of interest

The authors have no conflicts of interest to disclose.

Data available on request from the authors

The data that support the findings of this study are available from the corresponding author upon reasonable request.

REFERENCES

[1] G. Liger-Belair and C. Cilindre, Annual Rev. Anal. Chem. **14**, 21 (2021).
[2] G. Liger-Belair, M. Bourget, C. Cilindre, H. Pron, and G. Polidori, Journal of Food Engineering **116**, 78 (2013).
[3] R. Batt, J. Chem. Educ. **48**, 75 (1971).
[4] M. Vollmer and K.-P. Möllmann, Phys. Educ. **47**, 608 (2012).
[5] G. Liger-Belair, D. Cordier, J. Honvault, and C. Cilindre, Sci Rep **7**, 10938 (2017).
[6] G. Liger-Belair, D. Cordier, and R. Georges, Science Advances **5**, eaav5528 (2019).
[7] R. Campargue, The Journal of Physical Chemistry **88**, 4466 (1984).
[8] A. Potapov, A. Canosa, E. Jiménez, and B. Rowe, Angewandte Chemie International Edition **56**, 8618 (2017).
[9] M. Herman, T. Földes, K. Didriche, C. Lauzin, and T. Vanfleteren, International Reviews in Physical Chemistry **35**, 243 (2016).
[10] E. Mach and P. Salcher, *Optische Untersuchung Der Luftstrahlen* (F. Tempsky, 1890).

[11] H. Reichenbach, Annual Review of Fluid Mechanics **15**, 1 (1983).
[12] S.W. Kieffer, Nature **291**, 568 (1981).
[13] J.S. Méndez Harper, C. Cimarelli, J. Dufek, D. Gaudin, and R.J. Thomas, Geophysical Research Letters **45**, 7226 (2018).
[14] M.M. Orescanin, J.M. Austin, and S.W. Kieffer, Journal of Geophysical Research **115**, (2010).
[15] N.C. Shibley and G. Laughlin, Planet. Sci. J. **2**, 221 (2021).
[16] F.S. Sherman, (n.d.).
[17] J. von der Linden, C. Kimblin, I. McKenna, S. Bagley, H.-C. Li, R. Houim, C.S. Kueny, A. Kuhl, D. Grote, M. Converse, C.E.J. Vossen, S. Stern, C. Cimarelli, and J. Sears, Commun Earth Environ **2**, 195 (2021).
[18] M.M. Orescanin and J.M. Austin, Journal of Propulsion and Power (2012).
[19] N. Belouaggadia, H. Olivier, and R. Brun, J. Fluid Mech. **607**, 167 (2008).
[20] J. Pattison, S. Celotto, A. Khan, and W. O'Neill, Surface and Coatings Technology **202**, 1443 (2008).
[21] J.T. BATINA, AIAA j **28**, 1381 (1990).
[22] E. Rathakrishnan, *Applied Gas Dynamics* (John Wiley & Sons, 2019).
[23] L. Wagner and S. Braun, Numerical Investigation of the Gas Jet Formation Immediately after Opening a Champagne Bottle, PhD Thesis, Wien, 2021.
[24] J. Sinclair and X. Cui, Physics of Fluids **29**, 026102 (2017).